Mechanics of Materials 155 (2021) 103744

Contents lists available at ScienceDirect

Mechanics of Materials

journal homepage: www.elsevier.com/locate/mechmat

Hardening behaviour in the irradiated high entropy alloy

Qihong Fang [a], Jing Peng [a], Yang Chen [a], Li Li [a], Hui Feng [a], Jia Li [a,*], Chao Jiang [a,**], Peter K. Liaw [b]

[a] College of Mechanical and Vehicle Engineering, Hunan University, Changsha, 410082, PR China
[b] Department of Materials Science and Engineering, University of Tennessee, Knoxville, TN, 37996, USA

ARTICLE INFO

Keywords:
High-entropy alloy
Irradiation
Mechanical properties
Hardening mechanism
Crystal plasticity modeling

ABSTRACT

Due to the development and utilization of nuclear energy, there is an urgent need for metal materials that have stable mechanical properties under irradiation conditions. In recent years, high-entropy alloys (HEAs) have been widely concerned, and their excellent properties under extreme conditions have been explored, so that they are considered as candidate materials under nuclear fusion and fission conditions. However, modeling the irradiated hardening behaviour in HEA is still lacking. Here, considering the effect of severe lattice distortion, the hardening behavior of the irradiated FeNiMnCr HEA is investigated by the crystal plasticity theory. The results show that the yield strength of the irradiated FeNiMnCr HEA obtained by hardening model agrees well with the experimental data at the irradiation doses of 0 dpa, 0.03 dpa and 0.3 dpa. In addition, the relationship between the elemental concentrations and mechanical properties in FeNiMnCr HEA is discussed, revealing that the variation of Cr concentration has the greatest effect on yield stress. The FeNiMnCr HEA presents the larger yield strength when the Cr elemental fraction is 0.65. The modeling and results could provide an effective theoretical way to tune the yield strength and alloying design in advanced HEAs for meeting irradiation properties.

1. Introduction

In recent years, with the exploitation and utilization of nuclear energy, it is necessary to develop a new family of materials with better irradiation behavior. According to previous studies, high-entropy alloys (HEAs) are promising materials for application of nuclear energy because of their excellent mechanical properties and outstanding radiation resistance (Li et al., 2020a; George et al., 2019). Unlike most conventional alloys, whose primary properties are determined by one or two major elements, HEAs are consisted of four or more elements in equimolar or approximately equimolar amounts (Yeh et al., 2004). Therefore, the majority of HEAs have numerous excellent properties, such as high strength, high hardness, wear resistance, corrosion resistance, high temperature stability and electrical resistance (Xian et al., 2017; Miracle et al., 2017; Shi et al., 2017).

In addition, due to the difference in atomic size and shear modulus of each principal element, HEAs have unique severe lattice distortion effects, which make dislocation motion more difficult in HEAs than in conventional alloys (Miracle et al., 2017). Lattice distortion effects of HEAs are widely studied (Lee et al., 2018; Varvenne and Curtin, 2018; Li et al., 2020a,b; Toda-Caraballo and Rivera-Díaz-del-Castillo, 2015; Lee et al., 2020). Through first-principles method, it is found that the interatomic interaction and atomic size mismatch of refractory HEA can cause severe lattice distortion (Lee et al., 2018, 2020). HEAs are treated as a high-concentration solute-strengthened alloy, in which every constituent element is a "solute" in an "effective medium matrix", expressing the average alloy properties. Meantime, the yield strength of HEAs composed of arbitrary element at the finite strain-rate and the finite temperature can be predicted (Varvenne and Curtin, 2018). The model of solid solution hardening in HEA has been proposed (Toda-Caraballo and Rivera-Díaz-del-Castillo, 2015). The hardening effects of each atoms in complex alloys are obtained by comparing the results collected from the literature and theoretical data of the model, so that the homogeneous deformation and considerable strain hardening of HEA are explained. The model has the advantages of easy access to parameters and wide applicability which have been further verified by comparing the theoretical model results with molecular dynamics simulation results (Li et al., 2020b).

In the initial stage of irradiation, a large number of irradiation-induced defects, including interstitial atom and vacancy, are produced

* Corresponding author.
** Corresponding author.
E-mail addresses: lijia123@hnu.edu.cn (J. Li), jiangc@hnu.edu.cn (C. Jiang).

https://doi.org/10.1016/j.mechmat.2021.103744
Received 16 May 2020; Received in revised form 1 January 2021; Accepted 1 January 2021
Available online 6 January 2021

in metal materials subjected to the high-energy particle impact. Through atomic simulation and theory of diffusion kinematics (Aidhy et al., 2009), the point defects diffuse violently in the irradiation dynamics stage, some of the point defects are absorbed by the sinks originally existing in the material; and the other part of the saturated point defects aggregate with the diffusion and migration progress in order to become more stable and larger defect clusters, such as voids, stacking tetrahedrons and dislocation loops (Yang et al., 2018; Lu et al., 2018). These defects affect the movement and evolution of dislocations during the plastic deformation of irradiated metal materials. This trend leads to significant changes in the macroscopic mechanical properties of the materials (Lehtinen et al., 2018; Chen et al., 2018). From previous experiments (Zinkle and Snead, 2014; Tong et al., 2018), lattice distortion of HEAs can improve the defect pinning capability and hinder the accumulation of defects. There are less irradiation-induced segregations (RIS) in HEAs than conventional alloys (Kumar et al., 2016). In addition, the degree of swelling and irradiation damage has been found to decrease with the increase of compositional complexity (Zhang et al., 2015). The FeNiMnCr HEA exhibits excellent irradiation resistance and has lower defect cluster size and higher cluster density compared to conventional FeCrNi alloys. Its main irradiation-induced defects are dislocation loops (Kumar et al., 2016). In the past studies, irradiation hardening behaviors of HEAs are principally studied by experiments, however, few theoretical models are proposed to study the irradiated damage. Based on the results of experiment and simulation, analyzing the deformation mechanism and establishing the theoretical model for irradiation hardening are important to investigate the effect of irradiation hardening and predict the influence of irradiation-induced defects on the mechanical properties. Moreover, the crystal plasticity theory has not been used to study the HEAs, which is an effective method to combine the atomic-scale and dislocation-level process, and link them to the macroscopic deformation process. Therefore, the purpose of this paper is to propose an irradiation hardening model of FeNiMnCr HEA by crystal plasticity theory, for obtaining a more general application of this model in others HEAs.

In section 2, the irradiation hardening model is provided for describing the contributions of dislocation loops, lattice distortion and dislocation to the yield stress of FeNiMnCr HEA. In section 3, the rationality of the irradiation hardening model is verified through comparing with experimental data and theoretical data. In section 4, the influence of the atomic fraction of each component on the hardening of FeNiMnCr HEA is discussed, which provides a theoretical basis for the design of the HEAs.

2. Modeling details

2.1. Plasticity theoretical model

In this part, according to the classical crystal plasticity theory (Asaro and Rice, 1977), the clear theoretical frame of the face-centered cubic (FCC) single crystal FeNiMnCr HEA irradiated is presented under applied loads. In the elasto-viscoplastic constitutive equation, the elastic strain rate $\dot{\varepsilon}^e$ and viscoplastic strain rate $\dot{\varepsilon}^{vp}$ make up the total strain rate $\dot{\varepsilon}$:

$$\dot{\varepsilon} = \dot{\varepsilon}^e + \dot{\varepsilon}^{vp} \tag{1}$$

According to the law of Hooke, the elastic strain rate $\dot{\varepsilon}^e$ can be shown as:

$$\dot{\varepsilon}^e = \mathbb{S} : \dot{\sigma} \tag{2}$$

where $\mathbb{S}$ is elastic compliance tensor, which is the inverse of the elastic stiffness tensor $\mathbb{S} = \mathbb{C}^{-1}$, and $\dot{\sigma}$ denotes stress rate. The viscoplastic strain rate $\dot{\varepsilon}^{vp}$ is represented by Eq. (3),

$$\dot{\varepsilon}^{vp} = \sum_{\alpha=1}^{N_s} \mathbf{R}^\alpha \dot{\gamma}^\alpha \tag{3}$$

which is the cumulative result of the shear rate of every slip system. N_s is the overall number of slip systems and the number of FCC alloy slip system is 12. $\mathbf{R}^\alpha$is the Schmid tensor gotten by Eq. (4):

$$\mathbf{R}^\alpha = \frac{1}{2}(\mathbf{s}^\alpha \otimes \mathbf{n}^\alpha + \mathbf{n}^\alpha \otimes \mathbf{s}^\alpha) \tag{4}$$

$\mathbf{s}^\alpha$ and $\mathbf{n}^\alpha$ denote the slip direction and normal direction of the α slip system, respectively. $\dot{\gamma}^\alpha$ is the plastic shear rate on α slip system, and it can be expressed as:

$$\dot{\gamma}^\alpha = \dot{\gamma}_0 \left(\frac{|\tau^\alpha|}{\tau_c^\alpha} \right)^{\frac{1}{m}} \tag{5}$$

where $\dot{\gamma}_0$ and m are reference plastic shear rate and strain rate sensitivity coefficients, respectively (Peirce et al., 1982). τ^α represents the resolved shear stress (RSS) which denotes the relationship between the Schmid tensor and Cauchy stress via $\tau^\alpha = \mathbf{R}^\alpha : \boldsymbol{\sigma}$. τ_c^α is the critical resolved shear stress (CRSS).

By the Eqs. (1)–(5), the theoretical framework of crystal plasticity for single crystal is established. For irradiated HEAs, CRSS should involve the irradiation-induced defect hardening τ_d^α, the dislocation hardening τ_n^α, and the solid solution strengthening τ_{ss}, which is caused by lattice distortion. The effect of irradiation from dislocation hardening and the solid solution strengthening is not considered in the classic alloys (Xiao et al., 2016). According to the experimental study (Kumar et al., 2016), the main irradiation-induced defect in the FeNiMnCr HEA is the dislocation loop. The model of hardening mechanism can be vividly described in Fig. 1.

Hence, CRSS of the FeNiMnCr HEA can be expressed as:

$$\tau^\alpha = \tau_{ss} + \tau_n^\alpha + \tau_d^\alpha \tag{6}$$

where τ_{ss} is solid solution strengthening, τ_n^α is dislocation hardening, and τ_d^α is dislocation loop hardening.

2.2. Lattice distortion

In HEAs, the lattice distortion, which caused by the differences of shear modulus and atomic size between different type atoms (Lee et al., 2018), makes dislocation motion become more difficult. Its contribution to CRSS can be expressed by the following formula:

$$\tau_{ss} = t^{-1}\sigma_{ss} \tag{7}$$

where $t = 3.06$ is Taylor coefficient (Kumar et al., 2016). σ_{ss} is the resistance of dislocation motion owing to the lattice distortion. According to Vegard's law (Toda-Caraballo and Rivera-Díaz-del-Castillo, 2015), the solid solution strengthening of HEAs can be linked by the strengthening of a single element due to mismatch, as follows:

$$\sigma_{ss} = \sum_{i=1}^{n} c_i \sigma_{ss}^i \tag{8}$$

where n is the number of element types, and c_i is concentration (in atomic fraction) of the atom i. σ_{ss}^i is the mismatch strengthening of the atom i, which is the key to get the total mismatch strengthening of HEAs, and the expression can be shown as:

$$\sigma_{ss}^i = A\mu c_i^{2/3} \delta_i^{4/3} \tag{9}$$

where the parameter, A, is a material related constant, which has been explained by a statistical theory of solid solution hardening (Labusch, R. 1970). These research results (Lee et al., 2018; Li et al., 2020b) suggest

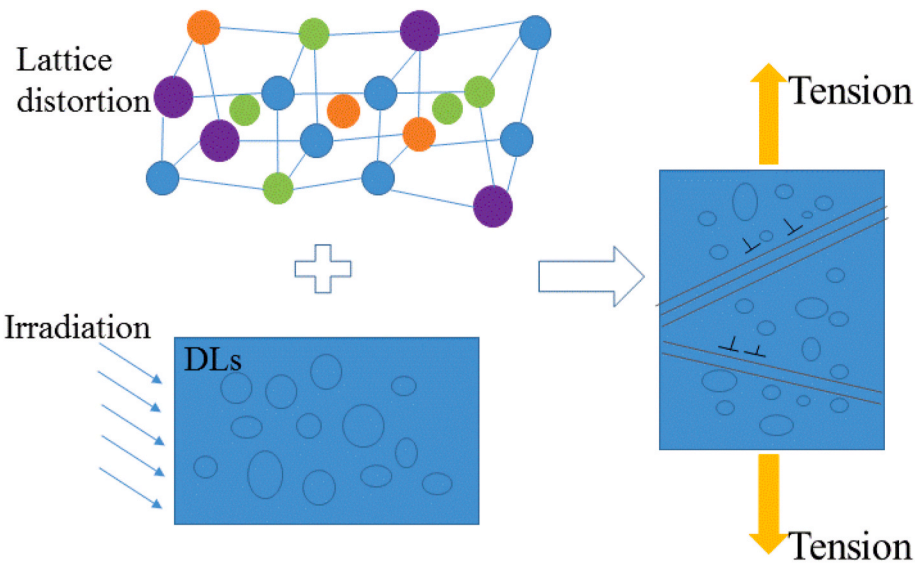

Fig. 1. The model of hardening mechanism. The severe lattice distortion, dislocation and irradiation-induced dislocation loops are considered in the model of HEAs.

that the value of A is 0.04. The mismatch parameter δ_i, in Eq. (9) can be written as (Toda-Caraballo and Rivera-Díaz-del-Castillo, 2015):

$$\delta_i = \xi\left(\delta\mu_i^2 + \beta^2\delta r_i^2\right)^{1/2} \tag{10}$$

where $\xi = 1$ in FCC metals, and $\xi = 4$ in BCC metals (Toda-Caraballo and Rivera-Díaz-del-Castillo, 2015), for the FCC HEA FeNiMnCr in this work, ξ is equal to 1. The value of β depends on the type of dislocation, for screw dislocations, $2 < \beta < 4$, and for edge dislocations, $\beta \geq 16$. In the present work, $\beta = 16$ because the edge dislocations are the primary dislocations type in FCC HEAs (Lee et al., 2018; Wang et al., 2017). μ is the shear modulus of the HEA which is related to shear modulus of each element and the atomic fraction. According to the Vegard's law, the shear modulus in Eq. (10) is shown as:

$$\mu = \sum_i^n c_i\mu_i \tag{11}$$

μ_i is shear modulus of i element. Besides, δr_i and $\delta\mu_i$ respectively are the atomic size mismatch and the modulus mismatch introduced by atom i. The atomic size mismatch and the modulus mismatch can be expressed as:

$$\delta r_i = \frac{\delta r_{ijkl}^{ave} - \delta r_{jkl}^{ave}}{c_i} \tag{12}$$

$$\delta\mu_i = \frac{\delta\mu_{ijkl}^{ave} - \delta\mu_{jkl}^{ave}}{c_i} \tag{13}$$

By analyzing the mismatch caused by the influence of single element in HEAs, it is assumed that the four-principal HEA *ijkl* is composed of three-principal-matrix *jkl* and the additional element *i*. The average atomic size mismatch of four-principal *ijkl* HEA δr_{ijkl}^{ave} and average atomic size mismatch of three-principal *jkl* alloy δr_{jkl}^{ave} can be obtained through Eq. (14). The average modulus mismatch of four-principal *ijkl* HEA $\delta\mu_{ijkl}^{ave}$ and average modulus mismatch of three-principal *jkl* alloy $\delta\mu_{jkl}^{ave}$ are calculated by Eq. (15).

$$\delta r^{ave} = \sum_i^n\sum_j^n c_i c_j \delta r_{ij} = (c_1, c_2, \cdots, c_n)\begin{pmatrix} \delta r_{11} & \delta r_{12} & \cdots & \delta r_{1n} \\ \delta r_{21} & \delta r_{22} & \cdots & \delta r_{2n} \\ \vdots & \cdots & \ddots & \vdots \\ \delta r_{n1} & \delta r_{n2} & \cdots & \delta r_{nn} \end{pmatrix}\begin{pmatrix} c_1 \\ c_2 \\ \vdots \\ c_n \end{pmatrix} \tag{14}$$

$$\delta\mu^{ave} = \sum_i^n\sum_j^n c_i c_j \delta\mu_{ij} = (c_1, c_2, \cdots, c_n)\begin{pmatrix} \delta\mu_{11} & \delta\mu_{12} & \cdots & \delta\mu_{1n} \\ \delta\mu_{21} & \delta\mu_{22} & \cdots & \delta\mu_{2n} \\ \vdots & \cdots & \ddots & \vdots \\ \delta\mu_{n1} & \delta\mu_{n2} & \cdots & \delta\mu_{nn} \end{pmatrix}\begin{pmatrix} c_1 \\ c_2 \\ \vdots \\ c_n \end{pmatrix} \tag{15}$$

where $\delta\mu_{ij}$ and δr_{ij} respectively indicate the modulus mismatch and the atomic size mismatch among the atom i and the atom j. It is easy to know that both $\delta\mu_{ii}$ and δr_{ii} are equal zero because there are no the modulus mismatch and the atomic size mismatch between the atoms i and i.

$$\delta r_{ij} = 2\left(r_i - r_j\right) / \left(r_i + r_j\right) \tag{16}$$

$$\delta\mu_{ij} = 2\left(\mu_i - \mu_j\right) / \left(\mu_i + \mu_j\right) \tag{17}$$

where μ_i and μ_j represent the shear moduli of i and j pure metal crystals, and they have different values at different temperatures. r_i and r_j are the atomic radii of i and j pure metal crystals, respectively.

Here, the resistance of lattice distortion to dislocation movement σ_{ss} can be obtained by the above derivation in HEAs.

2.3. Dislocation strengthening

The movement of dislocations on the slip system is hindered by other dislocations, and the contribution of dislocations to CRSS can be expressed as:

$$\tau_n^\alpha = b\mu\sqrt{h_n\rho_n^\alpha} \tag{18}$$

where b is the value of the Burgers vector. The shear modulus μ is obtained by Eq. (11). h_n is the hardening coefficient of dislocation. Considering the multiplication and annihilation, the evolution of dislocation density can be expressed as:

$$\dot{\rho}_n^\alpha = \dot{\gamma}\left[k_1\sqrt{\rho_n^\alpha} - k_2^\alpha(\dot{\varepsilon}, T)\rho_n^\alpha\right] \tag{19}$$

where $\dot{\varepsilon}$ is the applied strain rate, and the relationship between k_1 (multiplication coefficient) and k_2^α (annihilation coefficient) can be written as:

$$\frac{k_2^\alpha(\dot{\varepsilon}, T)}{k_1} = \frac{\chi b}{g^\alpha}\left[1 - \frac{kT}{D^\alpha b^3}\ln\left(\frac{\dot{\varepsilon}}{\varepsilon_0}\right)\right] \tag{20}$$

where ε_0, D^α, g^α, k, and χ are the reference strain rate, the drag stress, the

normalized activation energy, the Boltzmann constant, and the interaction parameter, respectively. Eq. (20) describes the nonlinear relationship between multiplication coefficient and annihilation coefficient which is related to temperature and applied strain rate. According to previous derivation (Beyerlein and Tomé, 2008), the annihilation mechanisms due to dislocation climbing and cross-slip are considered in Eq. (20).

2.4. Dislocation loops

Dislocation loops hinder the slip motion of dislocations, resulting in an increase of yield stress. Due to the 12 slip systems of FCC crystal, the defect-dislocation interaction model is used to characterize the spatial dependence of the dislocation loop and dislocation interaction.

$$\tau_d^\alpha = b\mu\sqrt{h_d\sum_{\beta=1}^{N_d}\mathbf{N}^\alpha:\mathbf{H}^\beta} \tag{21}$$

where h_d is the dislocation loop hardening coefficient, and $N_d = 4$ is the value of feature plane {111} for dislocation loop. $\mathbf{N}^\alpha = \mathbf{n}^\alpha \otimes \mathbf{n}^\alpha$, here, $\mathbf{n}^\alpha$ denotes the normal vector of slip plane, $\mathbf{H}^\beta$ is the second-order tensor describing the dislocation loop:

$$\mathbf{H}^\beta = 3d_1\rho_1\mathbf{M}^\beta \tag{22}$$

$$\mathbf{M}^\beta = \mathbf{I}^{(2)} - \mathbf{n}^\beta \otimes \mathbf{n}^\beta \tag{23}$$

where $\mathbf{I}^{(2)}$ is the unit tensor of second-order, and $\mathbf{n}^\beta$ is the normal vector of feature plane for dislocation loop. ρ_1 and d_1 are the initial number density and diameter of dislocation loops, respectively.

The crystal plasticity framework of polycrystal FeNiMnCr HEA is established by the self-consistent method based on the single crystal plasticity model (Sabar et al., 2002; Xiao et al., 2015).

3. Verification of the model

In this paper, the current model is used to study the irradiation hardening behavior of the single-phase FeNiMnCr HEA, which pays attention to the yield stress and flow stress at different irradiation doses. In the irradiated FeNiMnCr HEA, its main defect is dislocation loop under ion irradiation conditions (Kumar et al., 2016). The irradiation hardening model of FeNiMnCr HEA is verified by comparing the yield stress from the calculated data and experimental data at different irradiation doses (Kumar et al., 2016; Wu and Bei, 2015). The characteristics of each element are in Table 1 (Kumar et al., 2016; Salishchev et al., 2014). Here, the loading strain rate is $2.8 \times 10^{-4}s^{-2}$. The average grain size of FeNiMnCr HEA is 35 μm, and its initial dislocation density is $5\times 10^{14}m^{-2}$ from the experimental data (Kumar et al., 2016). The parameters of dislocation loops induced by irradiation are shown in Table 2 (Kumar et al., 2016), and other physical parameters are summarized in Table 3 (Xiao et al., 2016).

The solid solution strengthening caused by lattice distortion in HEAs is an important component of hardening mechanism, and its value is independent of the irradiation dose. By fitting relevant experimental data under different irradiation conditions, the strength coefficient of the dislocation interaction ($h_n = 0.02$), and the dislocation loop intensity coefficient ($h_d = 0.035$) are obtained, respectively. The stress-strain curves of FeNiMnCr HEA predicted by the theoretical model at different irradiation doses are shown in Fig. 2(a). The effects of dislocation loops enhance the yield stress and flow stress as the irradiation dose increases from 0 dpa to 0.3 dpa. It is assumed that for the same material, the initial dislocation density and the degree of lattice distortion are the same at the various radiation doses. In addition, the relationship between the strain and stress under three irradiation doses is shown in Fig. 2(b). It can be found that the time for FeNiMnCr HEA from elastic stage to plastic stage increases with the increase of irradiation dose, which is mainly dominated by the evolution of dislocation density affected by dislocation loop. In Fig. 2(c), the dislocation density proliferates slowly with the increase of irradiation. As a result, the irradiation-induced dislocation loop impedes the dislocation motion, which is the origin of the irradiation hardening of the FeNiMnCr HEA. On the other hand, this result leads to a certain increase in the ability to resist plastic deformation at irradiation condition. In Fig. 2(d), the yield stress of FeNiMnCr HEA is obtained by the current hardening model from Fig. 2(a), which agrees well with the experiment and theoretical calculation at various irradiation doses (Kumar et al., 2016). When the irradiation dose is 0 dpa, the hardening mechanism of the FeNiMnCr HEA only includes the first two parts of Eq. (6), i.e., lattice distortion and dislocation interaction (Fig. 2(d)). Hence, the irradiated hardening mechanism originates the lattice distortion, the dislocation interaction and the dislocation loop. Comparing to the CRSS at the irradiation doses of 0 dpa, 0.03 dpa and 0.3 dpa, it can be seen that the contribution of dislocation loop on the CRSS would be dominant with the increase of irradiation doses. It explains clearly why the degree of irradiation hardening can enhance at the high irradiation dose.

Table 1
Physical parameters of the constituent elements.

Parameter	Fe	Ni	Mn	Cr
Atomic radius (pm)	124	125	127	125
Shear modulus (GPa)	82	76	81	115
Atomic fraction (at%)	27.1	29.5	26.6	16.8

Table 2
Dislocation loop parameters in the ion irradiated FeNiMnCr HEA specimens.

Temperature (K)	Dose (dpa)	Mean loop diameter (nm)	Loop density (m^{-3})
293	0.03	2.98	7.3×10^{22}
293	0.3	3.23	1.5×10^{23}
400	10	4.66	1.9×10^{22}
500	3	4.13	7.1×10^{21}
500	10	4.32	9.4×10^{21}
600	10	5.21	6.7×10^{21}
700	10	5.45	4.3×10^{21}

Table 3
Parameters for the model of irradiated FeNiMnCr HEA.

Parameter	Definition	Value	Units
H	Annihilation coefficient	10	–
K_1	Kocks-Mecking parameter	2×10^9	m^{-1}
X	Interaction parameter	0.9	–
G	Normalized activation energy	9×10^3	–
K	Boltzmann constant	1.38×10^{-23}	$J \cdot K^{-1}$
D	Proportionality constant	10^4	MPa
B	Burger's vector length	0.257	nm
$\dot{\varepsilon}_0$	Reference rate	1×10^7	s^{-1}
$\dot{\gamma}_0$	Reference plastic strain rate	1×10^{-3}	s^{-1}
M	Strain rate sensitivity	0.05	–

4. Results and discussion

From the theoretical analysis in section 2, the lattice distortion effects in HEAs caused by the difference of atomic radius and shear modulus are closely related to the concentration of each component, so that the concentration changes of different principals have obvious effects on the mechanical properties of the FeNiMnCr HEA. The concentration of each element for HEA with better mechanical properties needs to be predicted. In the analysis of optimal component prediction, the effect of elemental concentration on irradiation-induced defects is not considered.

For the FeNiMnCr HEA, the atomic fraction of Cr is assumed as x, and

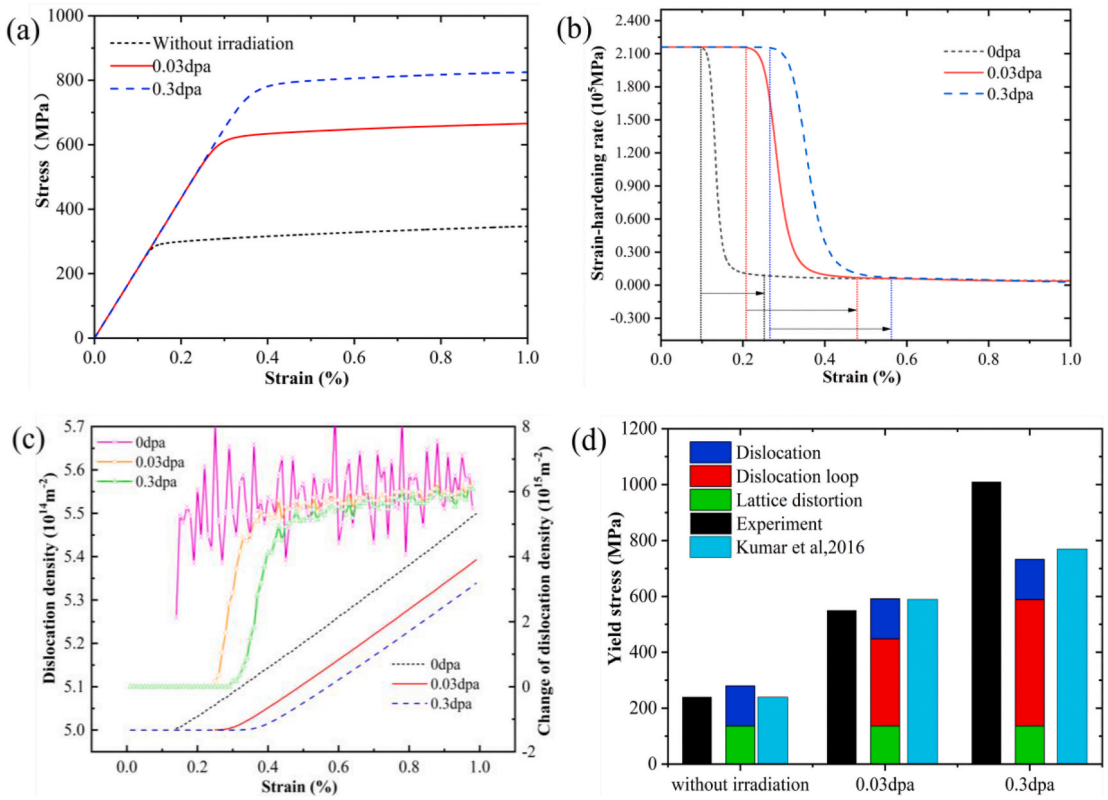

Fig. 2. Under irradiation doses of 0 dpa, 0.03 dpa and 0.3 dpa at 293 K, (a) stress-strain curves of the FeNiMnCr HEA, (b) strain-hardening rates, (c) evolutions of dislocation density with plastic deformation and variation of dislocation density at unit strain, (d) theoretical contributions of various hardening mechanisms to yield stress of FeNiMnCr HEA compared with the experimental data and theoretical data (Kumar et al., 2016).

the atomic fractions of Fe, Ni, and Mn are $(1-x)/3$, respectively. In Fig. 3(a), the contributions of three hardening mechanisms to yield stress are obtained at 293K under irradiation doses of 0 dpa, 0.03 dpa and 0.3 dpa by using the constitutive equation derived from section 2. When the atom fraction of Cr increases from 0.1 to 0.85, the variation of contribution of the solid solution strengthening to the yield stress is very significant, due to that the average atom size mismatch δr^{ave} and average modulus mismatch $\delta\mu^{ave}$ are obviously changed with the increase concentration of Cr. The value of the contribution is maximum when the Cr fraction is 0.65. The shear modulus of Cr is larger than that of other elements in the Table 1. Thus, the shear modulus in FeNiMnCr$_x$ HEA depends upon the trend of Cr fraction. The contributions of the dislocation hardening and the dislocation loop hardening gradually reinforce with the increase of Cr fractions (Fig. 3(a)). Additionally, due to the effect of irradiation on dislocation hardening and solid solution strengthening is not considered in this study, their contributions with the change of Cr concentration are basically approximate at each irradiation doses. However, the contributions of dislocation loop hardening to yield stress in FeNiMnCr$_x$ HEAs are different, due to the various densities and sizes of dislocation loops at different irradiation doses. The proportions of three hardening mechanisms on yield stress of FeNiMnCr$_x$ are shown in Fig. 3(b). The proportion of dislocation hardening increases firstly, and then decreases with the increase of Cr concentration.

In Fig. 4(a), the changes of yield stress from three hardening mechanisms are described at three different irradiation doses. The overall contribution of the three hardening mechanisms to yield stress reaches a maximum at the Cr fraction of 0.65. At $0 \le x \le 0.65$, three hardening mechanisms show an upward trend, and cause the increase of yield

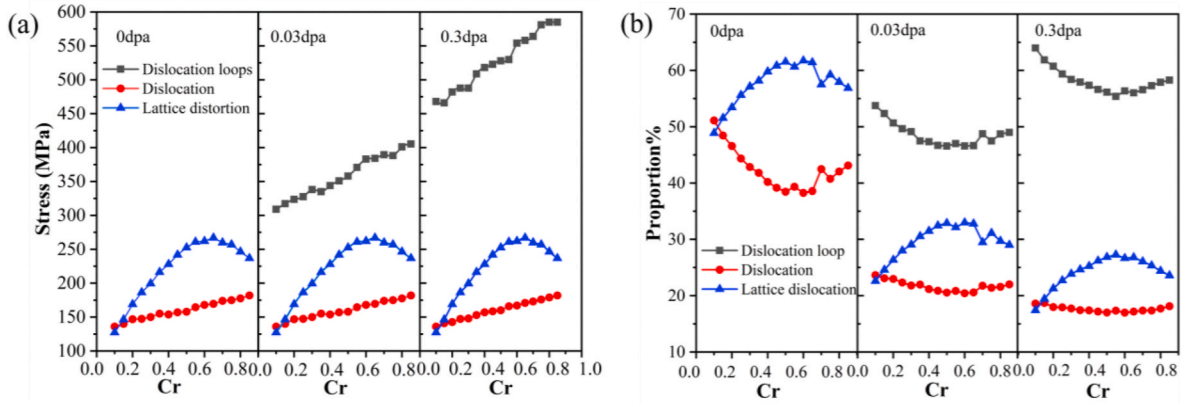

Fig. 3. (a) Contributions and (b) proportions of three hardening mechanisms to yield stress of FeNiMnCr$_x$ under 293 K and irradiation doses of 0 dpa, 0.03 dpa, and 0.3 dpa.

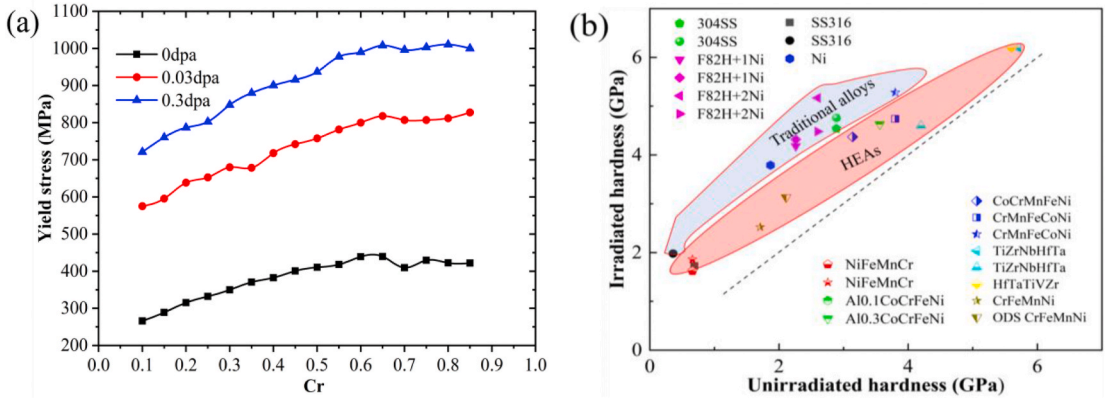

Fig. 4. (a) The yield stress vs. Cr element concentration for different irradiation doses. (b) Comparisons between irradiated hardness and unirradiated hardness in HEAs and traditional alloys, where the dotted line indicates that there is no change in hardness after irradiation.

stress. With the increase of Cr fraction from 0.65 to 0.85, the lattice distortion effect begins to gradually decreases in the $FeNiMnCr_x$ HEA. The yield stress remains basically unchanged when the Cr fraction exceeds 0.65. This indicates that the lattice distortion dominated by Cr fraction has a significant effect on hardening compared to dislocation hardening and dislocation loop hardening. Besides, in Fig. 4(b), comparisons of irradiated hardness and non-irradiated hardness in HEAs and traditional alloys reveal that the radiation hardening resistance of HEAs is generally more excellent than that of traditional alloys (Li et al., 2020a). Hence, the severe lattice distortion in HEAs would play a critical role in enhancing the radiation resistance in a comparison of the traditional alloys.

In addition, the effects of Fe, Ni and Mn on yield stress in the FeNiMnCr HEA are investigated, as shown in the Fig. 5. The contributions of three hardening mechanisms in $Fe_xNiMnCr$, $FeNi_xMnCr$ and $FeNiMn_xCr$ HEAs are described at the irradiation condition of 0.3dpa and 293 K in Fig. 5(a). It suggests that both dislocation hardening and dislocation loop hardening decrease due to the decline of the shear modulus for all three HEAs (according to Eq. (17), and the shear modulus of Fe, Ni, and Mn are much less than Cr from Table 1). The changes of the yield stress in $Fe_xNiMnCr$, $FeNi_xMnCr$ and $FeNiMn_xCr$ HEAs are described in Fig. 5(b). By comparing Figs. 4(a) and Fig. 5(b), the most significant effect of Cr on the yield stress is found in the FeNiMnCr HEA, which is helpful for the design of new HEAs with good radiation resistance. Moreover, the maximum yield stresses of $FeNiMnCr_x$ HEAs at different irradiation doses of 0 dpa, 0.03 dpa and 0.3 dpa are predicted by our theoretical model, which are 439 MPa, 818 MPa and 1008 MPa at Cr fraction of 0.65, respectively. This is due to that the highest lattice distortion and higher dislocation loop hardening in $FeNiMnCr_x$ HEAs appear at $x = 0.65$.

5. Conclusions

In this work, considering three hardening mechanisms of lattice distortion, dislocation and dislocation loop, an irradiation hardening model is brought forward for studying the irradiation hardening behavior of FeNiMnCr HEA at the different irradiation doses of 0 dpa, 0.03 dpa and 0.3 dpa. Comparing with theoretical data and experiment in the FeNiMnCr HEA, the hardening model proposed is proved to be suitable for the HEAs. The contribution of dislocation loop to irradiation hardening strengthens with increasing irradiation dose due to the proliferation of mean dislocation loop diameter and density. The dislocation loop hardening is the main source of radiation hardening. The difficulty of dislocation slip is increased due to the generation of dislocation loop induced by irradiation. This trend makes the dislocation proliferate slowly, and then the time from elastic stage to plastic stage increases in FeNiMnCr HEA. By comparing the effects of Fe, Ni, Mn, and Cr fraction on the yield stress, the increase of Cr fraction has higher influence on the hardening, and the degree of lattice distortion hardening is the maximum when the Cr fraction reaches 0.65. This research could provide an effective theoretical way to guide alloying design of other advanced HEAs for meeting irradiation properties.

Declaration of competing interest

The authors declare that they have no known competing financial

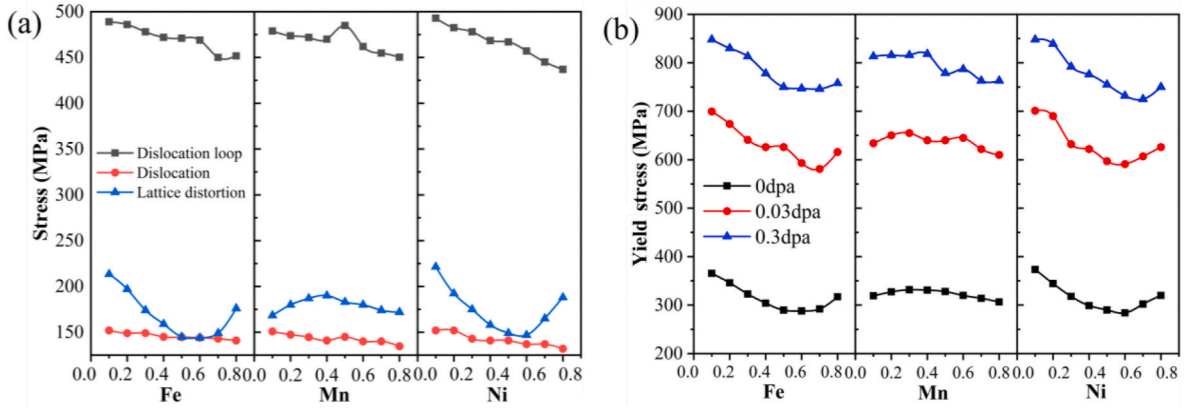

Fig. 5. (a) The stress contributed from various hardening mechanisms for the element concentration in $Fe_xNiMnCr$, $FeNi_xMnCr$ and $FeNiMn_xCr$ HEAs under irradiation doses of 0.3 dpa. (b) The yield stress vs. the element concentration for different irradiation doses.

interests or personal relationships that could have appeared to influence the work reported in this paper.

Acknowledgements

The authors would like to deeply appreciate the supports from the Foundation for Innovative Research Groups of the National Natural Science Foundation of China (Grant No. 51621004), the National Natural Science Foundation of China (51871092, and 11772122), the State Key Laboratory of Advanced Design and Manufacturing for Vehicle Body (71865015).

References

Aidhy, D.S., Millett, P.C., Wolf, D., Phillpot, S.R., Huang, H., 2009. Kinetically driven point-defect clustering in irradiated MgO by molecular-dynamics simulation. Scripta Mater. 60 (8), 691–694.

Asaro, R.J., Rice, J.R., 1977. Strain localization in ductile single crystals. J. Mech. Phys. Solid. 25 (5), 309–338.

Beyerlein, I.J., Tomé, C.N., 2008. A dislocation-based constitutive law for pure Zr including temperature effects. Int. J. Plast. 24 (5), 867–895.

Chen, W.Y., Liu, X., Chen, Y., Yeh, J.W., Tseng, K.K., Natesan, K., 2018. Irradiation effects in high entropy alloys and 316H stainless steel at 300° C. J. Nucl. Mater. 510, 421–430.

George, E.P., Raabe, D., Ritchie, R.O., 2019. High-entropy alloys. Nat. Rev. Mater. 4 (8), 515–534.

Kumar, N.K., Li, C., Leonard, K.J., Bei, H., Zinkle, S.J., 2016. Microstructural stability and mechanical behavior of FeNiMnCr high entropy alloy under ion irradiation. Acta Mater. 113, 230–244.

Labusch, R., 1970. A statistical theory of solid solution hardening. Phys. Status Solidi B 41 (2), 659–669.

Lee, C., Chou, Y., Kim, G., Gao, M.C., An, K., Brechtl, J., Zhang, C., Chen, W., Poplawsky, J.D., Song, G., Ren, Y., Chou, Y., Liaw, P.K., 2020. Lattice-distortion-enhanced yield strength in a refractory high-entropy alloy. Adv. Mater. 32 (49), 2004029.

Lee, C., Song, G., Gao, M.C., Feng, R., Chen, P., Brechtl, J., Chen, Y., An, K., Guo, W., Poplawsky, J.D., Li, S., Samaei, A.T., Chen, W., Hu, A., Choo, H., Liaw, P.K., 2018. Lattice distortion in a strong and ductile refractory high-entropy alloy. Acta Mater. 160, 158–172.

Lehtinen, A., Laurson, L., Granberg, F., Nordlund, K., Alava, M.J., 2018. Effects of precipitates and dislocation loops on the yield stress of irradiated iron. Sci. Rep. 8 (1), 6914.

Li, J., Fang, Q., Liaw, P.K., 2020a. Microstructures and properties of high-entropy materials: modeling, simulation, and experiments. Adv. Eng. Mater., 2001044

Li, J., Li, L., Jiang, C., Fang, Q., Liu, F., Liu, Y., Liaw, P.K., 2020b. Probing deformation mechanisms of gradient nanostructured CrCoNi medium entropy alloy. J. Mater. Sci. Technol. 57, 85–91.

Lu, C., Yang, T., Jin, K., Velisa, G., Xiu, P., Song, M., Peng, Q., Gao, F., Zhang, Y., Bei, H., Weber, W.J., Wang, L., 2018. Enhanced void swelling in NiCoFeCrPd high-entropy alloy by indentation-induced dislocations. Mater. Res. Lett. 6 (10), 584–591.

Miracle, D.B., Senkov, O.N., 2017. A critical review of high entropy alloys and related concepts. Acta Mater. 122, 448–511.

Peirce, D., Asaro, R.J., Needleman, A., 1982. An analysis of nonuniform and localized deformation in ductile single crystals. Acta Metall. 30 (6), 1087–1119.

Sabar, H., Berveiller, M., Favier, V., Berbenni, S., 2002. A new class of micro–macro models for elastic–viscoplastic heterogeneous materials. Int. J. Solid Struct. 39 (12), 3257–3276.

Salishchev, G.A., Tikhonovsky, M.A., Shaysultanov, D.G., Stepanov, N.D., Kuznetsov, A. V., Kolodiy, I.V., Tortika, A.S., Senkov, O.N., 2014. Effect of Mn and V on structure and mechanical properties of high-entropy alloys based on CoCrFeNi system. J. Alloys Compd. 591, 11–21.

Shi, Y., Yang, B., Liaw, P., 2017. Corrosion-resistant high-entropy alloys: a review. Metals 7 (2), 43.

Toda-Caraballo, I., Rivera-Díaz-del-Castillo, P.E., 2015. Modelling solid solution hardening in high entropy alloys. Acta Mater. 85, 14–23.

Tong, Y., Velisa, G., Zhao, S., Guo, W., Yang, T., Jin, K., Lu, C., Bei, H., Ko, J.Y.P., Pagan, D.C., Zhang, Y., Wang, L., Zhang, F.X., 2018. Evolution of local lattice distortion under irradiation in medium-and high-entropy alloys. Materialia 2, 73–81.

Varvenne, C., Curtin, W.A., 2018. Predicting yield strengths of noble metal high entropy alloys. Scripta Mater. 142, 92–95.

Wang, Z., Li, J., Fang, Q., Liu, B., Zhang, L., 2017. Investigation into nanoscratching mechanical response of AlCrCuFeNi high-entropy alloys using atomic simulations. Appl. Surf. Sci. 416, 470–481.

Wu, Z., Bei, H., 2015. Microstructures and mechanical properties of compositionally complex Co-free FeNiMnCr18 FCC solid solution alloy. Mater. Sci. Eng. 640, 217–224.

Xian, X., Zhong, Z., Zhang, B., Song, K., Chen, C., Wang, S., Cheng, J., Wu, Y., 2017. A high-entropy V35Ti35Fe15Cr10Zr5 alloy with excellent high-temperature strength. Mater. Des. 121, 229–236.

Xiao, X., Song, D., Xue, J., Chu, H., Duan, H., 2015. A self-consistent plasticity theory for modeling the thermo-mechanical properties of irradiated FCC metallic polycrystals. J. Mech. Phys. Solid. 78, 1–16.

Xiao, X., Terentyev, D., Yu, L., Bakaev, A., Jin, Z., Duan, H., 2016. Investigation of the thermo-mechanical behavior of neutron-irradiated Fe-Cr alloys by self-consistent plasticity theory. J. Nucl. Mater. 477, 123–133.

Yang, T., Xia, S., Guo, W., Hu, R., Poplawsky, J.D., Sha, G., Fang, Y., Yan, Z., Wang, C., Li, C., Zhang, Y., Zinkle, S.J., Zhang, Y., 2018. Effects of temperature on the irradiation responses of Al0. 1CoCrFeNi high entropy alloy. Scripta Mater. 144, 31–35.

Yeh, J.W., Chen, S.K., Lin, S.J., Gan, J.Y., Chin, T.S., Shun, T.T., Tsau, C.H., Chang, S.Y., 2004. Nanostructured high-entropy alloys with multiple principal elements: novel alloy design concepts and outcomes. Adv. Eng. Mater. 6 (5), 299–303.

Zhang, Y., Stocks, G.M., Jin, K., Lu, C., Bei, H., Sales, B.C., Wang, L., Béland, L.K., Stoller, R.E., Samolyuk, G.D., Caro, M., Caro, A., Weber, W.J., 2015. Influence of chemical disorder on energy dissipation and defect evolution in concentrated solid solution alloys. Nat. Commun. 6, 8736.

Zinkle, S.J., Snead, L.L., 2014. Designing radiation resistance in materials for fusion energy. Annu. Rev. Mater. Res. 44, 241–267.